Analytical Modeling and Experimental Verification of the Vibrations of the Zigzag Microstructure for Energy Harvesting

M. Amin Karami[1]
e-mail: karami@vt.edu

Daniel J. Inman

Center for Intelligent Materials Systems and Structures,
Virginia Tech,
310 Durham Hall,
Blacksburg, VA 24061

This paper addresses an issue in energy harvesting that has plagued the potential use of harvesting through the piezoelectric effect at the micro-electro-mechanical systems (MEMS) scale. Effective energy harvesting devices typically consist of a cantilever beam substrate coated with a thin layer of piezoceramic material and fixed with a tip mass tuned to resonant at the dominant frequency of the ambient vibration. The fundamental natural frequency of a beam increases as its length decreases, so that at the MEMS scale the resonance condition occurs orders of magnitude higher than ambient vibration frequencies, rendering the harvester ineffective. Here, we propose a new geometry for MEMS scale cantilever harvesters with low fundamental frequencies. A "zigzag" geometry is proposed, modeled, and solved to show that such a structure would be able to vibrate near resonance at the MEMS scale. An analytical solution is presented and verified against Rayleigh's method and is validated against a macroscale experiment. The analysis is used to provide design guidelines and parametric studies for constructing an effective MEMS scale energy harvesting device in the frequency range common to low frequency ambient vibrations, removing a current barrier. [DOI: 10.1115/1.4002783]

1 Introduction

Cantilever type energy harvesting devices use a substrate to support a piezoelectric transduction element. The power output of such devices is maximum when the fundamental frequency is near the dominant frequency of ambient vibration, ensuring a resonance response maximizing the strain in piezoelectric materials. The high natural frequencies of the existing designs of MEMS vibrational energy harvesters are due to their short length constraint and present a serious drawback in the development of MEMS scale energy harvesting devices.

The topic of energy harvesting has been of great interest in the recent literature as well as in applications for wireless sensing. Several recent reviews of the literature are given in Refs. [1–6]. Our focus here is on the mechanics of the substrate and on how to lower the fundamental frequency to useful levels. The coupling of the mechanical and electrical fields is well explained in Refs. [7,8] and will not be repeated here.

The first design of a MEMS harvester was proposed by Lu et al. [9], where the thickness of the energy harvesting beam was one-tenth of its length. The dimension ratio seemed intuitive, dealing with large scale structures, but it was too large for a microcantilever and caused the beam's fundamental natural frequency to be about 3 kHz. The larger the deflection of the energy harvesting beam is, the more power is extracted. Therefore, the beams should be designed at or near their natural frequencies. The frequencies of typical ambient vibrations are from 1 Hz to 100 Hz. Having a natural frequency in orders of kilohertz simply means that the ambient vibration would not shake the structure at all. The improper choice of thickness to length ratio has resulted in similar frequencies in Refs. [10,11]. Zheng and Xu [12] used two beams, one with a distance on top of the other to support the tip mass. The configuration of the beams would make the structure very stiff and light, which translates to an even higher natural frequency (10 kHz).

Fang et al. [13] were the first to try a low thickness to length ratio (1/100). This resulted in a tremendous improvement in the natural frequency (600 Hz). The trend was followed by Refs. [14–18], and natural frequencies of about 460 Hz, 100 Hz, 971 Hz, 180 Hz, and 256 Hz were correspondingly achieved. This is still not low enough in many situations. What seems to be needed is an improvement in the general design of the harvester. The cantilever beam fundamental frequency is dependent on its length and cannot be designed to a lower frequency in a MEMS device because of space limitations. Spiral beams have been suggested as an alternative geometry [19], but since their vibrations are dominantly torsional [20], use of spirals for energy harvesting requires a complicated electrode configuration. Passive magnetic force can be used to contract the elastic force and reduce the natural frequency [21].

In order to produce a low frequency MEMS harvesting device, we propose using a zigzag structure depicted in Fig. 1. The superiority of the proposed shape over that of a simple cantilever beam can be explained based on a static deflection analysis (a rigorous calculation follows in Sec. 6). The deflection of the zigzag structure (Fig. 2(*b*)) due to the tip force at the end would be three times the deflection of the single cantilevered beam under the same load (Fig. 2(*a*)). The corresponding maximum bending moments in the two structures are identical, and therefore the necessary thickness of the zigzag structure is just the same as the necessary thickness of a single beam. Additional compliance can be realized by increasing the length of the single beam, but the longer the beam is, the thicker it should be to sustain the same load resulting in some reduction in compliance.

In the following, details of the zigzag design are given followed by an analysis of the coupled bending-torsion vibrations of the

[1]Corresponding author.

Contributed by the Technical Committee on Vibration and Sound of ASME for publication in the JOURNAL OF VIBRATION AND ACOUSTICS. Manuscript received December 15, 2009; final manuscript received May 31, 2010; published online December 8, 2010. Assoc. Editor: Dane Quinn.

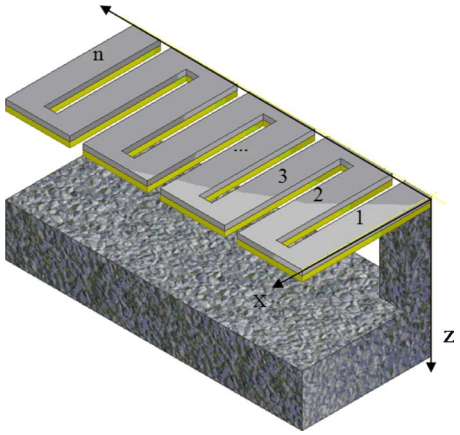

Fig. 1 The zigzag energy harvesting structure

structure. The governing partial differential equations are treated using separation of variables and are finally reduced to an eigenvalue problem. Solving the eigenvalue problem gives the natural frequencies and mode shapes of the structure. The relationship between the natural frequencies and the number of elements reveals the benefits of the proposed zigzag design for MEMS applications. The validity of the proposed analytical model is confirmed by approximating the fundamental natural frequency with Rayleigh's method and by experimental verification. The results of both case studies are close to the predictions of the analytical model.

2 Device Configuration

The structure of interest here is a flat zigzag spring illustrated in Fig. 1. The thin spring is fixed at one end and forms a cantilever structure. The plane that the zigzag structure lies in is called *the main plane* of the zigzag structure. The structure can deflect out of the main plane and can be modeled as a few straight beams, with rectangular cross sections, placed next to each other on the main plane. Each beam is connected to its neighbor beams at its ends. Each of the beams can bend out of the main plane and can twist. The portions of the structure that connect the elements are very small and are modeled here as rigid links. The torsion of each of the beams causes the next beam to move out of the main plane. The amount of relative motion is the torsion angle times the rigid arm length.

Each of the beams is a uniform composite beam composed of a piezoelectric layer bonded to the substructure layer (this forms a unimorph). The substructure can be made of silicon oxynitride, which results in a residual stress free microstructure.

When the beams are deflected, some strain is generated in the piezoelectric layer, which generates electrical energy.

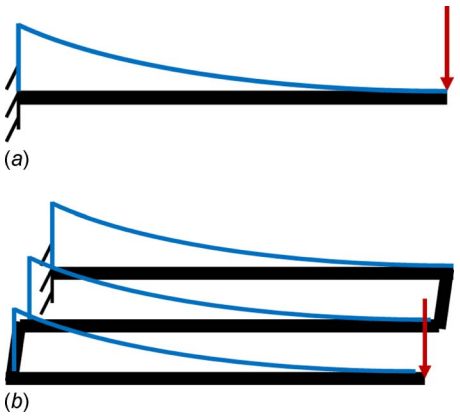

Fig. 2 Bending moment diagrams for (*a*) cantilevered beam and (*b*) zigzag structure

3 Governing Equations for Free Vibration Analysis

The structure can deflect in two ways: Each of the beams can bend, resulting in the deflection of that member and change in the start position of the next beams. The beams can also twist. The twist of each of the members does not affect the elevation of the points on that member but will lower or raise the next member. The amount of elevation (or decrease) is equal to the twist angle of the member times the distance between the two consequent beams.

The deformation of the beams can be quantified with their twist angle, $\beta_i(x,t)$, and out of plane displacement, $w_i(x,t)$. The index i identifies each beam. Both β_i and w_i are time dependent and vary along the beam and are therefore functions of x and t (refer to Fig. 1).

To derive the equivalent bending stiffness of the composite beam [7], we define

$$h_{pa} = \frac{h_p^2 + \frac{2Y_s h_p H_s}{Y_p} + \frac{Y_s h_s^2}{Y_p}}{2\left(h_p + Y_s \frac{h_s}{Y_p}\right)}, \quad h_{sa} = \frac{h_p^2 + 2h_p h_s + \frac{y_s h_s^2}{Y_p}}{2\left(h_p + Y_s \frac{h_s}{Y_p}\right)}$$

$$h_a = -h_{sa}, \quad h_b = h_{pa} - h_p, \quad h_c = h_{pa}$$

Then, the equivalent bending stiffness YI is calculated as (here, we use YI rather than the traditional EI to be compatible with the harvesting literature)

$$YI = b\left[\frac{Y_s(h_b^3 - h_a^3) + Y_p(h_c^3 - h_p^3)}{3}\right] \tag{1}$$

Since the thickness to length ratio of MEMS energy harvesters is typically 1/100, the classical Euler–Bernoulli assumptions are made. The validity of the assumptions can be checked by experimental verification. The equation of motion for the free vibration of an Euler–Bernoulli beam is [22]

$$YI\frac{\partial^4 w_i}{\partial x^4} + \rho A\frac{\partial^2 w_i}{\partial t^2} = 0$$

ρA is mass per unit length of the beam and equals

$$\rho A = b(\rho_s h_s + \rho_p h_p)$$

A standard separation of variables solution is substituted next:

$$w_i(x,t) = W_i(x)\,\eta(t)$$

This results in the general solution

$$W_i(x) = \sum_{j=1}^{4} A_{ij} e^{s_{ij}x} \tag{2}$$

where the exponents are derived as

$$s_{ij} = \pm\sqrt{\frac{\omega_n}{c}}, \quad \pm i\sqrt{\frac{\omega_n}{c}}, \quad j = 1,2,\ldots,4, \quad c = \sqrt{\frac{YI}{\rho A}} \tag{3}$$

The torsional equation of motion for the same beam is

$$GJ\frac{\partial^2 \beta_i}{\partial x^2} - I_p\frac{\partial^2 \beta_i}{\partial t^2} = 0$$

where GJ is the equivalent torsional rigidity of the thin composite beam [23,24] and is equal to

$$GJ = 3\frac{\frac{4(G_p h_p^3 + G_s h_s^3)}{3} - \frac{(G_p h_p^2 - G_s h_s^2)^2}{G_p h_p + G_s h_s}}{(h_p + h_s)^3} \times \frac{(h_s + h_p)^3 b^3}{3(b^2 + (h_s + h_p)^2)}$$

I_p is the mass axial moment of inertia of the beam per unit length about the axis of torsion and is approximated with

$$I_p \approx \frac{\rho_p}{12} b h_p (b^2 + h_p^2 + 3h_s^2) + \frac{\rho_s}{12} b h_s (b^2 + 3h_p^2 + h_s^2)$$

A separation of variables solution of the torsional equation is

$$\beta_i(x,t) = B_i(x)\,\eta(t)$$

This results in the general solution for the torsion,

$$B_i(x) = \sum_{j=5}^{6} A_{ij} e^{s_{ij} x} \tag{4}$$

where the exponents are

$$s_{ij} = \pm i\frac{\omega_n}{g}, \quad j = 5,6, \quad g = \sqrt{\frac{GJ}{I_p}} \tag{5}$$

Although in Eqs. (2) and (4) $W_i(x)$ and $B_i(x)$ are real functions, A_{ij} and s_{ij} are complex numbers. One can pair the complex exponents and their complex conjugates and continue dealing with real coefficients. We prefer to keep the complex form to keep the uniformity of the formulation. In the end, if all the calculations are performed correctly, we should get complex conjugate pairs for A_{ij}, which result in real $W_i(x)$ and $B_i(x)$.

4 Boundary, Equilibrium, and Continuity Conditions

There are six unknown coefficients, A_{ij}, for each of the beams. This therefore requires $6n$ relations to identify the free vibrations. Six boundary conditions are known for the two ends of the structure. There are six following equilibrium and continuity equations for each of the $n-1$ element interfaces. This gives additional $6(n-1)$ equations, and there will be a total of $6\times n$ equations for evaluating $6n$ unknown coefficients.

The following relations for the bending moment, shear force, and twist torque have been used in writing natural boundary conditions:

$$M(x,t) = -YI\frac{\partial^2 w(x,t)}{\partial x^2}, \quad Q(x,t) = -YI\frac{\partial^3 w(x,t)}{\partial x^3},$$

$$T(x,t) = GJ\frac{\partial \beta(x,t)}{\partial x}$$

4.1 Boundary Conditions for the Complete Structure. The total structure has a cantilever configuration, which means that one side of the structure is clamped and the other side is free. The essential boundary conditions at the clamped end are on the beam deflection, slope, and twist angle.

The beam deflection condition is

$$w_1(0,t) = 0 \Rightarrow W_1(0) = 0 \Rightarrow \sum_{j=1}^{4} A_{1j} e^{s_{1j}0} = 0$$

which can be written in matrix form for convenience as

$$\begin{bmatrix} 1 & 1 & 1 & 1 & 0 & 0 \end{bmatrix} \begin{bmatrix} A_{11} \\ \vdots \\ A_{16} \end{bmatrix} = 0 \tag{6}$$

The beam slope condition becomes

$$W_1'(0) = 0 \tag{7}$$

Lastly, the twist angle condition is

$$B_1(0) = \sum_{j=5}^{6} A_{1j} e^{s_{1j}0} = 0 \tag{8}$$

Equations (6)–(8) can be written as a single matrix relation:

$$[\boldsymbol{BC0}]_{3\times 6} \begin{bmatrix} A_{11} \\ \vdots \\ A_{16} \end{bmatrix} = \mathbf{0} : [\boldsymbol{BC0}]_{3\times 6} = \begin{bmatrix} 1 & 1 & 1 & 1 & 0 & 0 \\ s_{11} & s_{12} & s_{13} & s_{14} & 0 & 0 \\ 0 & 0 & 0 & 0 & 1 & 1 \end{bmatrix} \tag{9}$$

The x-coordinate of the free end of the structure can be either 0 or l depending on the number of zigzag members. In the following, x_{end} refers to the x-coordinate of the free end. The natural boundary conditions at the free end of the structure are as follows:

The moment balance condition for the free end is

$$M_n(x_{\text{end}}) = 0 \Rightarrow W_n''(x_{\text{end}}) = 0 \tag{10}$$

The shear force balance becomes $Q_n(x_{\text{end}}) = \pm m_{\text{tip}}[\partial^2 w_n(x_{\text{end}},t)/\partial t^2]$: The plus sign corresponds to $x_{\text{end}}=0$, and the minus sign corresponds to $x_{\text{end}}=l$. This can be written as

$$YIW_n^{(3)}(x_{\text{end}}) = \mp m_{\text{tip}}\omega^2 W_n(x_{\text{end}}) \tag{11}$$

The torque balance condition is

$$T_n(x_{\text{end}}) = 0 \Rightarrow B_n'(x_{\text{end}}) = 0 \tag{12}$$

Equations (10)–(12) combine to yield a single matrix equation

$$[\boldsymbol{BCe}]_{3\times 6} \begin{bmatrix} A_{n1} \\ \vdots \\ A_{n6} \end{bmatrix} = \mathbf{0}$$

where the $[\boldsymbol{BCe}]_{3\times 6}$ is defined as

$$[\boldsymbol{BCe}]_{3\times 6} = \begin{bmatrix} s_{n1}^2 e^{s_{n1}x_{\text{end}}} & s_{n2}^2 e^{s_{n2}x_{\text{end}}} & s_{n3}^2 e^{s_{n3}x_{\text{end}}} & s_{n4}^2 e^{s_{n4}x_{\text{end}}} & 0 & 0 \\ (YIs_{n1}^3 \pm m\omega^2) e^{s_{n1}x_{\text{end}}} & (YIs_{n2}^3 \pm m\omega^2) e^{s_{n2}x_{\text{end}}} & (YIs_{n3}^3 \pm m\omega^2) e^{s_{n3}x_{\text{end}}} & (YIs_{n4}^3 \pm m\omega^2) e^{s_{n4}x_{\text{end}}} & 0 & 0 \\ 0 & 0 & 0 & 0 & s_{n5} e^{s_{n5}x_{\text{end}}} & s_{n6} e^{s_{n6}x_{\text{end}}} \end{bmatrix} \tag{13}$$

4.2 Interface Equilibrium and Continuity Conditions. Each of the beams can be connected to the next beam either at their beginning, $x=0$, or at their end, $x=l$. For ease of reference, the location of the connection is named x^*, which can be either 0 or l depending on the side of connection.

As depicted in Fig. 3, the deflection continuity condition can be written as

$$W_i(x^*) = d \times B_{i-1}(x^*) + W_{i-1}(x^*) \tag{14}$$

This expression effectively couples the bending and torsional vibrations. The equation shows that the bending deflection of the ith element is affected by both the deflection and the twist angle of the previous element.

The slope continuity condition is

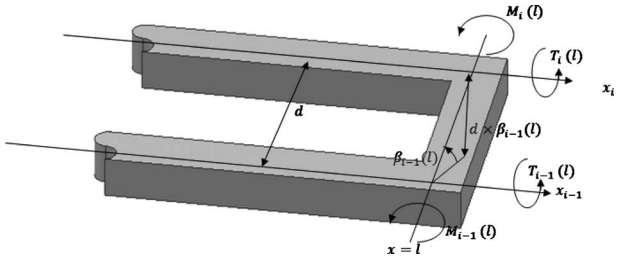

Fig. 3 Equilibrium and compatibility conditions

$$W_i'(x^*) = W_{i-1}'(x^*) \tag{15}$$

The twist angle continuity condition is

$$B_{i-1}(x^*) = B_i(x^*) \tag{16}$$

The bending moment equilibrium condition is

$$M_{i-1}(x^*) = -M_i(x^*) \Rightarrow W_i''(x^*) = -W_{i-1}''(x^*) \tag{17}$$

The shear force equilibrium condition is

$$Q_{i-1}(x^*) = -Q_i(x^*) \pm m_l \ddot{w}_i(x^*,t) \tag{18}$$

where the plus sign in the right hand side corresponds to $x^*=0$ and the minus sign is associated with $x^*=l$. Equation (18) can be written as

$$YIW_{i-1}^{(3)}(x^*) = -YIW_i^{(3)}(x^*) \mp m_l\omega^2 W_i(x^*) \tag{19}$$

The torque equilibrium condition is

$$T_{i-1} = -T_i + Q_i \times d \quad \text{or}$$

$$GJB_{i-1}'(x^*) = -GJB_i'(x^*) - YIW_i^{(3)}(x^*) \times d \tag{20}$$

This last expression reveals the second reason for coupled torsion-bending vibrations. The torque acting on one element is related to the twisting torque of the other element and the shear force at the other element's end.

Equations (14)–(20) can be written as a single matrix relation

$$[\boldsymbol{L_{i-1}}]_{6\times 6}\begin{bmatrix} A_{(i-1)1} \\ \vdots \\ A_{(i-1)6} \end{bmatrix} = [\boldsymbol{R_i}]_{6\times 6}\begin{bmatrix} A_{i1} \\ \vdots \\ A_{i6} \end{bmatrix} \tag{21}$$

where

$$\boldsymbol{L_{i-1}} = \begin{bmatrix} e^{s_{(i-1)1}x^*} & e^{s_{(i-1)2}x^*} & e^{s_{(i-1)3}x^*} & e^{s_{(i-1)4}x^*} & de^{s_{(i-1)5}x^*} & de^{s_{(i-1)6}x^*} \\ s_{(i-1)1}e^{s_{(i-1)1}x^*} & s_{(i-1)2}e^{s_{(i-1)2}x^*} & s_{(i-1)3}e^{s_{(i-1)3}x^*} & s_{(i-1)4}e^{s_{(i-1)4}x^*} & 0 & 0 \\ 0 & 0 & 0 & 0 & e^{s_{(i-1)5}x^*} & e^{s_{(i-1)6}x^*} \\ -s_{(i-1)1}^2 e^{s_{(i-1)1}x^*} & -s_{(i-1)2}^2 e^{s_{(i-1)2}x^*} & -s_{(i-1)3}^2 e^{s_{(i-1)3}x^*} & -s_{(i-1)4}^2 e^{s_{(i-1)4}x^*} & 0 & 0 \\ -s_{(i-1)1}^3 e^{s_{(i-1)1}x^*} & -s_{(i-1)2}^3 e^{s_{(i-1)2}x^*} & -s_{(i-1)3}^3 e^{s_{(i-1)3}x^*} & -s_{(i-1)4}^3 e^{s_{(i-1)4}x^*} & 0 & 0 \\ 0 & 0 & 0 & 0 & GJs_{(i-1)5}e^{s_{(i-1)5}x^*} & GJs_{(i-1)6}e^{s_{(i-1)6}x^*} \end{bmatrix}$$

$$\boldsymbol{R_i} = \begin{bmatrix} e^{s_{i1}x^*} & e^{s_{i2}x^*} & e^{s_{i3}x^*} & e^{s_{i4}x^*} & 0 & 0 \\ s_{i1}e^{s_{i1}x^*} & s_{i2}e^{s_{i2}x^*} & s_{i2}e^{s_{i2}x^*} & s_{i4}e^{s_{i4}x^*} & 0 & 0 \\ 0 & 0 & 0 & 0 & e^{s_{i5}x^*} & e^{s_{i6}x^*} \\ s_{i1}^2 e^{s_{i1}x^*} & s_{i2}^2 e^{s_{i2}x^*} & s_{i3}^2 e^{s_{i3}x^*} & s_{i4}^2 e^{s_{i4}x^*} & 0 & 0 \\ \left(\pm\frac{m_l\omega^2}{YI} + s_{i1}^3\right)e^{s_{i1}x^*} & \left(\pm\frac{m_l\omega^2}{YI} + s_{i2}^3\right)e^{s_{i2}x^*} & \left(\pm\frac{m_l\omega^2}{YI} + s_{i3}^3\right)e^{s_{i3}x^*} & \left(\pm\frac{m_l\omega^2}{YI} + s_{i4}^3\right)e^{s_{i4}x^*} & 0 & 0 \\ dYIs_{i1}^3 e^{s_{i1}x^*} & dYIs_{i2}^3 e^{s_{i2}x^*} & dYIs_{i3}^3 e^{s_{i3}x^*} & dYIs_{i4}^3 e^{s_{i4}x^*} & GJs_{i5}e^{s_{i5}x^*} & GJs_{i6}e^{s_{i6}x^*} \end{bmatrix}$$

5 Eigenvalue Problem

So far, we have elaborated the boundary, continuity, and equilibrium conditions. These conditions will result in an eigenvalue problem as typically encountered in studying vibrations of continuous systems [25]. There are two different formulations possible. The first approach is to write all the derived conditions as follows:

$$[\boldsymbol{M}]_{6n\times 6n}[A_{11},\ldots,A_{16},A_{21},\ldots,A_{26},\ldots,A_{n1},A_{n6}]^T = \mathbf{0}_{6n\times 1} \tag{22}$$

Since the trivial solution is unacceptable, we must have $\det(\boldsymbol{M}_{6n\times 6n})=0$. Matrix $\boldsymbol{M}$ is a function of geometry (x_{end} and x^*) and the roots of a characteristic equation (s_{ij}). The s_{ij} are, in turn, functions of natural frequency through Eqs. (3) and (5). Therefore, for a given geometry, the $\det(\boldsymbol{M})$ is only a function of ω_n. The values of ω_n, which make $\det(\boldsymbol{M})=0$, are the natural frequencies of the structure. Substituting the natural frequencies in Eq. (24), we can evaluate $A_{11}-A_{n5}$ for a given A_{n6}. These coefficients define the mode shapes corresponding to each natural frequency.

The alternative approach is to use Eq. (21) to write all the constants A_{ij} in terms of constants of the first element, A_{1j}. Equation (21) gives

$$\begin{bmatrix} A_{i1} \\ \vdots \\ A_{i6} \end{bmatrix} = \boldsymbol{R_i^{-1}L_{i-1}}\begin{bmatrix} A_{(i-1)1} \\ \vdots \\ A_{(i-1)6} \end{bmatrix}$$

Similarly, we have

$$\begin{bmatrix} A_{n1} \\ \vdots \\ A_{n6} \end{bmatrix} = \boldsymbol{R_n^{-1}L_{n-1}}\begin{bmatrix} A_{(n-1)1} \\ \vdots \\ A_{(n-1)6} \end{bmatrix} = \boldsymbol{R_n^{-1}L_{n-1}R_{n-1}^{-1}L_{n-2}}\begin{bmatrix} A_{(n-2)1} \\ \vdots \\ A_{(n-2)6} \end{bmatrix}$$

This enables us to go ahead and relate the coefficients of the last beam to those of the first member as

Table 1 The specifications of the beams

Length of the beams, l (mm)	10
Width of each of the beams, b (mm)	1
Center to center lateral distance of two adjacent beams, d (mm)	1.5
Thickness of the piezoelectric layer, h_p (μm)	20
Thickness of the substructure, h_s (μm)	25
Tip mass (mgr)	26.7
Young's modulus of the piezoelectric layer, Y_p (GPa)	66
Young's modulus of the Si_2N_2O substructure, Y_s (GPa) [28]	140
Modulus of rigidity of the piezoelectric layer, G_p (GPa)	25
Modulus of rigidity of the substructure, G_s (GPa)	38
Density of the piezoelectric layer, ρ_p (kg m^{-3})	7800
Density of the substructure, ρ_s (kg m^{-3})	4400

$$\begin{bmatrix} A_{n1} \\ \vdots \\ A_{n6} \end{bmatrix} = \boldsymbol{R}_n^{-1}\boldsymbol{L}_{n-1}\boldsymbol{R}_{n-1}^{-1}\boldsymbol{L}_{n-2}\ldots\boldsymbol{R}_2^{-1}\boldsymbol{L}_1 \begin{bmatrix} A_{11} \\ \vdots \\ A_{16} \end{bmatrix} \tag{23}$$

Equations (9), (13), and (23) imply that

$$\begin{bmatrix} \boldsymbol{BC0}_{3\times 6} \\ \boldsymbol{BCe}_{3\times 6}[\boldsymbol{R}_n^{-1}\boldsymbol{L}_{n-1}\boldsymbol{R}_{n-1}^{-1}\boldsymbol{L}_{n-2}, \ldots, \boldsymbol{R}_2^{-1}\boldsymbol{L}_1]_{6\times 6} \end{bmatrix}_{6\times 6} \begin{bmatrix} A_{11} \\ \vdots \\ A_{16} \end{bmatrix} = \boldsymbol{0}_{6\times 1} \tag{24}$$

The matrix $\boldsymbol{N}$ is accordingly defined as

$$\boldsymbol{N} = \begin{bmatrix} \boldsymbol{BC0} \\ \boldsymbol{BCeR}_n^{-1}\boldsymbol{L}_{n-1}\boldsymbol{R}_{n-1}^{-1}\boldsymbol{L}_{n-2}, \ldots, \boldsymbol{R}_2^{-1}\boldsymbol{L}_1 \end{bmatrix}_{6\times 6}$$

Equation (24) gives a nontrivial solution if and only if $\det(\boldsymbol{N})=0$, providing the values of ω_n, which make $\det(\boldsymbol{N})=0$. In finding the mode shapes, we substitute derived natural frequencies in Eq. (24) and evaluate A_{11}–A_{15} for a given A_{16}. After $[A_{11},\ldots,A_{16}]^T$ is evaluated, other coefficients can be calculated from the following formula. The mode shapes can subsequently be constructed knowing all the constants from

$$\begin{bmatrix} A_{i1} \\ \vdots \\ A_{i6} \end{bmatrix} = \boldsymbol{R}_i^{-1}\boldsymbol{L}_{i-1}\boldsymbol{R}_{i-1}^{-1}\boldsymbol{L}_{i-2}, \ldots, \boldsymbol{R}_2^{-1}\boldsymbol{L}_1 \begin{bmatrix} A_{11} \\ \vdots \\ A_{16} \end{bmatrix}$$

The great advantage of the eigenvalue formulation (Eq. (23)) is the significantly reduced size of the coefficient matrix. The size of $\boldsymbol{M}$ is $6n\times 6n$, while the size of $\boldsymbol{N}$ is only 6×6. Therefore, calculating $\det(\boldsymbol{M})$ is numerically intensive compared with the calculation of $\det(\boldsymbol{N})$. Also, the value of $\det(\boldsymbol{M})$ can sometimes be in order of 10^{200}, while the equivalent $\det(\boldsymbol{N})$ is about 10^{20}. The extremely large value of $\det(\boldsymbol{M})$ can introduce numerical errors in finding natural frequencies. Therefore, we utilize the second approach to find natural frequencies and mode shapes.

6 Free Vibration Results

In this section, we use the proposed analytical method to calculate the natural frequencies and the mode shapes of a zigzag structure. The dimensions and material properties of the structure, depicted in Fig. 1, are given in Table 1.

Based on the above analysis, Fig. 4 is constructed for various numbers of elements in the zigzag pattern. Figure 4 illustrates that by increasing the number of elements, we can decrease the first five natural frequencies of the structure by an order of magnitude. In the study, the dimensions of the beams composing the structure are fixed and are given in Table 1. The number of members in the structure varies from 1 to 20, and the tip mass is equal to the mass of one member. The natural frequencies of the structures with different numbers of beams have been calculated. The decrease in the fundamental natural frequency is approximately exponential with the slope of −20 dB/decade, which means that the fundamental natural frequency drops by one order if the number of beams increases by an order of magnitude.

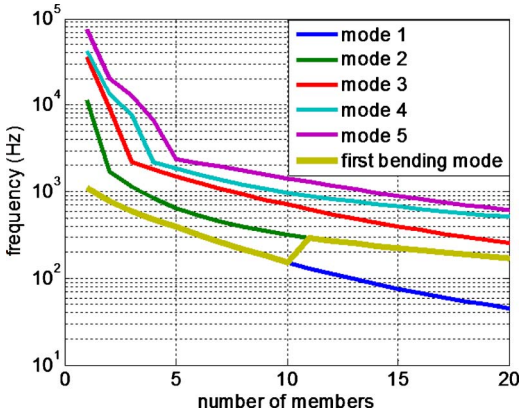

Fig. 4 Natural frequency relation with the number of members

The fundamental mode shape of a single cantilevered beam corresponds to the bending of the beam. As the number of elements increases, the natural frequency of the modes, which involve torsion of the beams, decreases faster than the natural frequency of the modes related to the bending of the members. In an energy harvesting application, the electrodes are placed on top and bottom surfaces of the piezoelectric layers. This means that the electrical energy is produced only from the bending of the piezoelectric layer and not from torsion. As we are mainly concerned about the vibrations that result in voltage generation, we should be concerned with the change in the natural frequency of the first bending mode and not with that in the fundamental natural frequency. If the structure has more than ten members, the fundamental mode shape becomes dominantly torsional. This means that we would get more power from the second mode than from the fundamental mode. The first bending mode would therefore be the second. This suggests using a zigzag structure composed of less than ten members unless we are forced by the frequency requirement to use more members.

The other advantage of using the zigzag geometry for energy harvesting is that as we increase the number of members, the natural frequencies get closer together; the ratio of the fifth natural frequency over the first one is about 70 for a single beam, while it reduces to 10 for a ten-member structure. This advantage can be used for broadband energy harvesting. This conclusion on the number of elements is specific to the illustrated case. In general, adding the tip mass allows having more beams before making the fundamental mode dominantly tensional. In contrast, the larger the distance between the beams, the less number or members we can have.

For illustration, the first four mass normalized mode shapes of a ten-member structure are plotted in Fig. 5. We can distinguish the torsional modes from the bending modes from their corresponding mode shapes. In torsional modes, the beams are flat and the elevation of each beam is different from the previous one due to the torsion of the previous beam. The slope of connecting arms and the lack of curvature of beams are the main two characteristic features.

In bending modes, the beams are no longer flat. They are slightly curved, which indicates that the beams are bending. Moreover, the connecting arms are almost flat, indicating that the torsion in the members is insignificant. In the illustrated mode shapes, the first mode depicted in Figs. 5(*a*) and 5(*b*) is torsional. The next modes plotted in Figs. 5(*c*) and 5(*d*), Figs. 5(*e*) and 5(*f*), and Figs. 5(*g*) and 5(*h*) are dominantly bending. In the higher

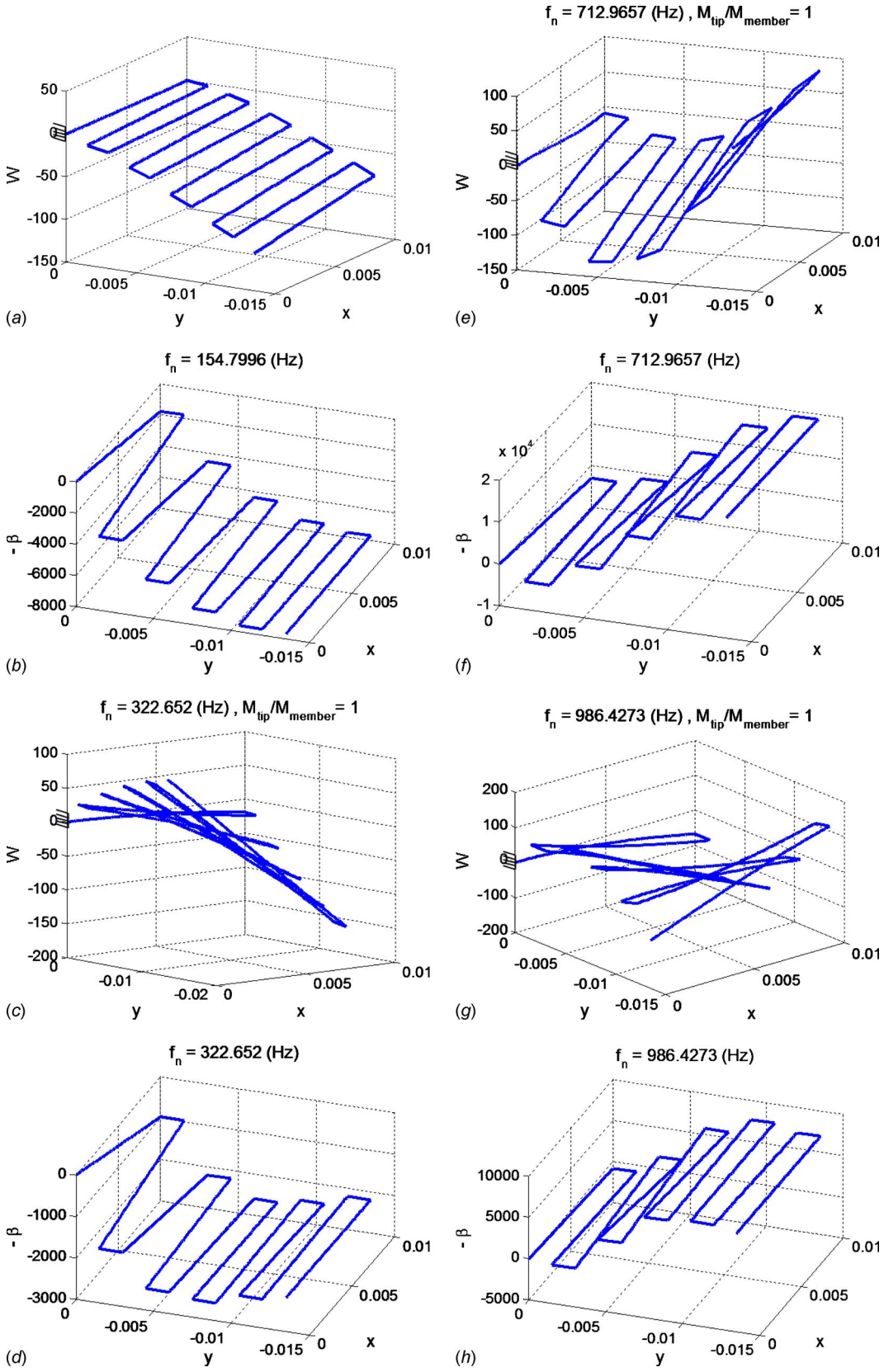

Fig. 5 (*a*)–(*h*) **Mass normalized mode shapes of the first four modes**

modes of the same structure (an example is plotted in Fig. 6), the coupling between torsion and bending is more significant, and both contribute to the deflection of the structure.

The mode shapes are an excellent means to examine if the boundary conditions and the continuity and equilibrium conditions have been truly satisfied. It can be confirmed that for all the mode shapes, the out of plane deflection W, its derivative, and the twist angle β are zero at the fixed end of the structure. W, dW/dx,

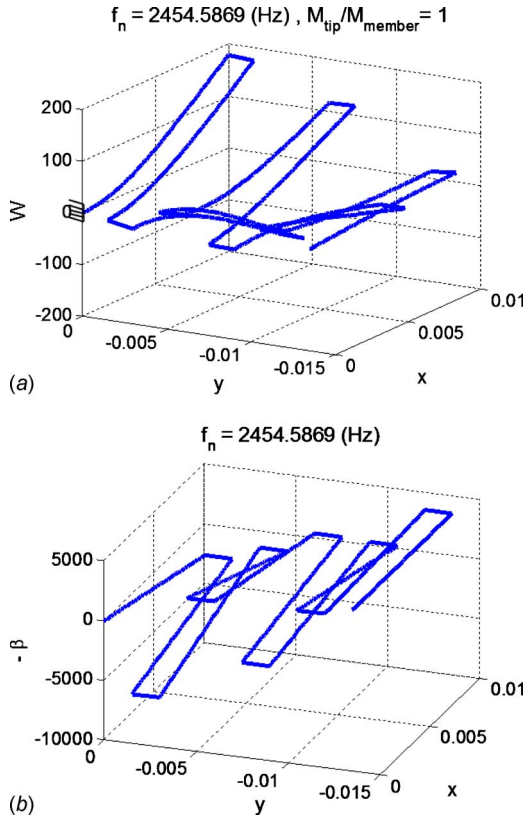

Fig. 6 (*a*) and (*b*) Mode shape of the tenth mode

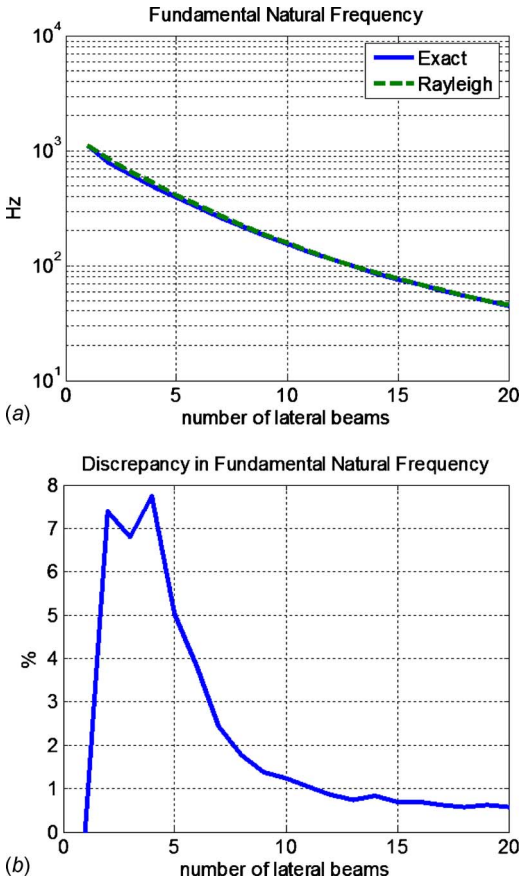

Fig. 7 The exact versus the approximate fundamental frequencies

and β at the ends of any two connected beams match at their point of junction. Although it is difficult to see in the plots, it was also determined that the curvature of the beam and the slope of the β curve at the free end are zero, which confirms that the natural boundary conditions are satisfied.

7 Vibration Analysis Using Rayleigh's Method

Rayleigh's method is commonly used to approximate the fundamental natural frequency of structures. Here, we use Rayleigh's quotient to calculate the fundamental natural frequency of several structures for comparison with our exact model as a check. The frequency that resulted from Rayleigh's method is always greater than the exact fundamental frequency [26] but should be close to that frequency provided that the trial function is close to the fundamental mode shape. Considering the bending and torsional deflection of beams, we can calculate the strain energy in the structure as [27]

$$\pi = \sum_{i=1}^{n} \frac{EI}{2} \int_0^L \left(\frac{\partial^2 w_i}{\partial x^2} \right)^2 dx + \sum_{i=1}^{n} \frac{GJ}{2} \int_0^L \left(\frac{\partial \beta_i}{\partial x} \right)^2 dx \tag{25}$$

The kinetic energy associated with the out of plane deflection of the beam is

$$T_e = \frac{1}{2} \sum_{i=1}^{n} \int_{x=0}^{L} \rho A \left(\frac{\partial w_i}{\partial t} \right)^2 dx + \frac{1}{2} \sum_{i=1}^{n-1} m_l \left(\frac{\partial w_i(x^*)}{\partial t} \right)^2 + \frac{m_{\text{tip}}}{2} \left(\frac{\partial w_i(x_{\text{end}})}{\partial t} \right)^2 \tag{26}$$

Having chosen a trial function $\psi_i(x)$, by separating the variables as $w_i(x,t) = \psi_i(x)\,\eta(t)$ and assuming harmonic vibrations such that $\dot{\eta} = i\omega\eta$, we finally derive the natural frequency as

$$\omega^2 = \frac{\Sigma_{i=1}^{n} \int_0^L (EI(\psi_i'')^2 + GJ(\beta_i')^2) dx}{\Sigma_{i=1}^{n} \rho A \int_0^L \psi_i^2 dx + M_{\text{tip}} \psi_n^2(x_{\text{end}}) + \Sigma_{i=1}^{n-1} m_l \psi_i^2(x^*)} \tag{27}$$

The static deflection curve of the structure under its own weight is used as the trial function. This choice is well known to result in good approximates of the fundamental frequency of elastic structures [22]. To find the static deflection shape under gravity, we start from the tip of the structure where we know that the shear force, the twist torque, and the bending moment are zero. We add up the effects of the point force due to the tip mass and the distributed force resulting from the distributed mass of the beam to find the values of the shear force, bending moment, and twist torque along the last beam and its junction to the neighboring beam. Next, Eqs. (17), (18), and (20) can be used to calculate the force and moments at the tip of the next neighboring member. The procedure described is repeated until forces and moments are calculated along the members and at the junctions. Then, we use the known force and moments to calculate the deflected shape under gravity. This deflection curve is used as the trial function, $\psi_i(x)$, in Eq. (27) to find the approximate fundamental natural frequency.

The fundamental natural frequency of the structure discussed in Sec. 6 has been calculated using the exact method and Rayleigh's method. The results are illustrated in Fig. 7. The estimation from Rayleigh's method is close to the exact fundamental frequency, and as expected the approximate frequency is always higher than the exact value. The maximum discrepancy is about 8%, which corresponds to the four-member structure.

8 Experimental Verification

Experimental measurements have been performed as a second validation of the analytical model. To avoid the expense of MEMS

Table 2 The specifications of the experimental structures

Length of the beams, l (mm)	171.4
Width of each of the beams, b (mm)	19
Center to center lateral distance of two adjacent beams, d (mm)	22.2
Thickness of the substructure, h_s (mm)	4.76
Tip mass (including accelerometer) (gr)	7.8
Young's modulus of aluminum 5083, Y_s (GPa)	73.1
Density of the aluminum substructure, ρ_s (kg m^{-3})	2770

fabrication, a macrosize model of the zigzag structure has been tested. The structure is described in Table 2 and illustrated in Fig. 8.

To characterize the vibrations, the accelerations of the base and the tip of the structure are measured using two accelerometers. Considering the presented analytical solution, the transfer function between the base and the tip motion can be derived after performing a modal expansion,

$$w_i(x,t) = \phi_{i(m)}(x)\,\eta_{(m)}(t) \tag{28}$$

where $\phi_{i(m)}(x)$ is the mass normalized mode shape, i.e.,

$$\sum_{i=1}^{n}\int_0^L \rho A\,\phi_{i(m)}^2(x)dx + \sum_{i=1}^{n-1} m_l\phi_{i(m)}^2(x^*) + m_{\text{tip}}\phi_{n(m)}^2(x_{\text{end}}) = 1 \tag{29}$$

The base vibrations, exciting the structure, are in and out of the main plane. Therefore, the governing differential equations for the deflection of the structure relative to its base are

$$YI\frac{\partial^4 w_{i(\text{rel})}}{\partial x^4} + \rho A\frac{\partial^2 w_{i(\text{rel})}}{\partial t^2} = -\left[\rho A + m_{\text{tip}}\delta(x - x_{\text{end}})\,\delta(i-n) + \sum_{i=1}^{n-1} m_l\delta(x - x^*)\right] a_b(t)$$

$$GJ\frac{\partial^2\beta_i}{\partial x^2} - I_p\frac{\partial^2\beta_i}{\partial t^2} = 0 \tag{30}$$

Substituting Eq. (28) in Eq. (30), taking the Fourier transform, premultiplying by $\phi_{i(r)}(x)$, and integrating over all the structure results to

$$\frac{\eta_{\text{rel}}(\omega)}{a_b(\omega)} = -\sum_{r=1}^{\infty}\frac{\gamma_r}{\omega_r^2 + 2j\zeta_r\omega_r\omega - \omega^2} \tag{31}$$

where γ_r is defined as

$$\gamma_r = \sum_{i=1}^{n}\int_0^L \phi_{i(m)}(x) + \sum_{i=1}^{n-1} m_l\phi_{i(m)}(x^*) + m_{\text{tip}}\phi_{n(m)}(x_{\text{end}}) \tag{32}$$

The relative tip acceleration is related to the base acceleration as

$$\frac{a_{\text{rel}}(\omega)}{a_b(\omega)} = \sum_{r=1}^{\infty}\frac{\gamma_r\phi_r(x_{\text{end}})\omega^2}{\omega_r^2 + 2j\zeta_r\omega_r\omega - \omega^2} \tag{33}$$

Figure 9 illustrates the values derived from Eq. (33) and the values from the experiments for 1-, 3-, 5-, 8-, and 11-member structures. The experiments show that the fundamental natural frequencies of the structures are correspondingly 142.2 Hz, 58.28 Hz, 29.75 Hz, 14.19 Hz, and 8.18 Hz. Therefore, the fundamental natural frequency of an 11-member structure is less than 1/17 of that of a cantilever beam with the same thickness and beam length.

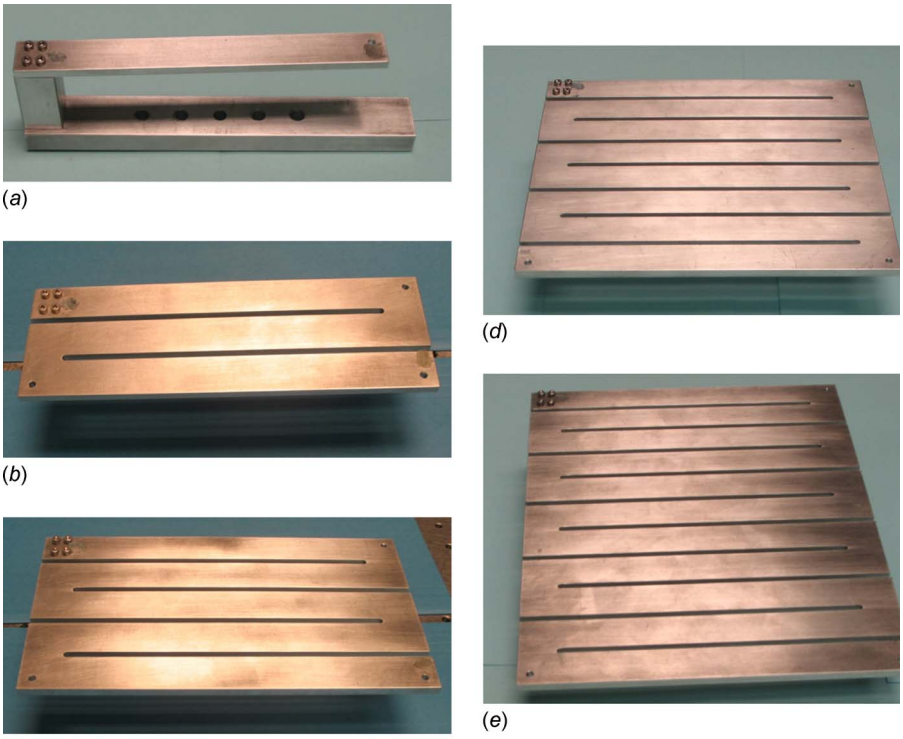

Fig. 8 Experimental zigzag structures

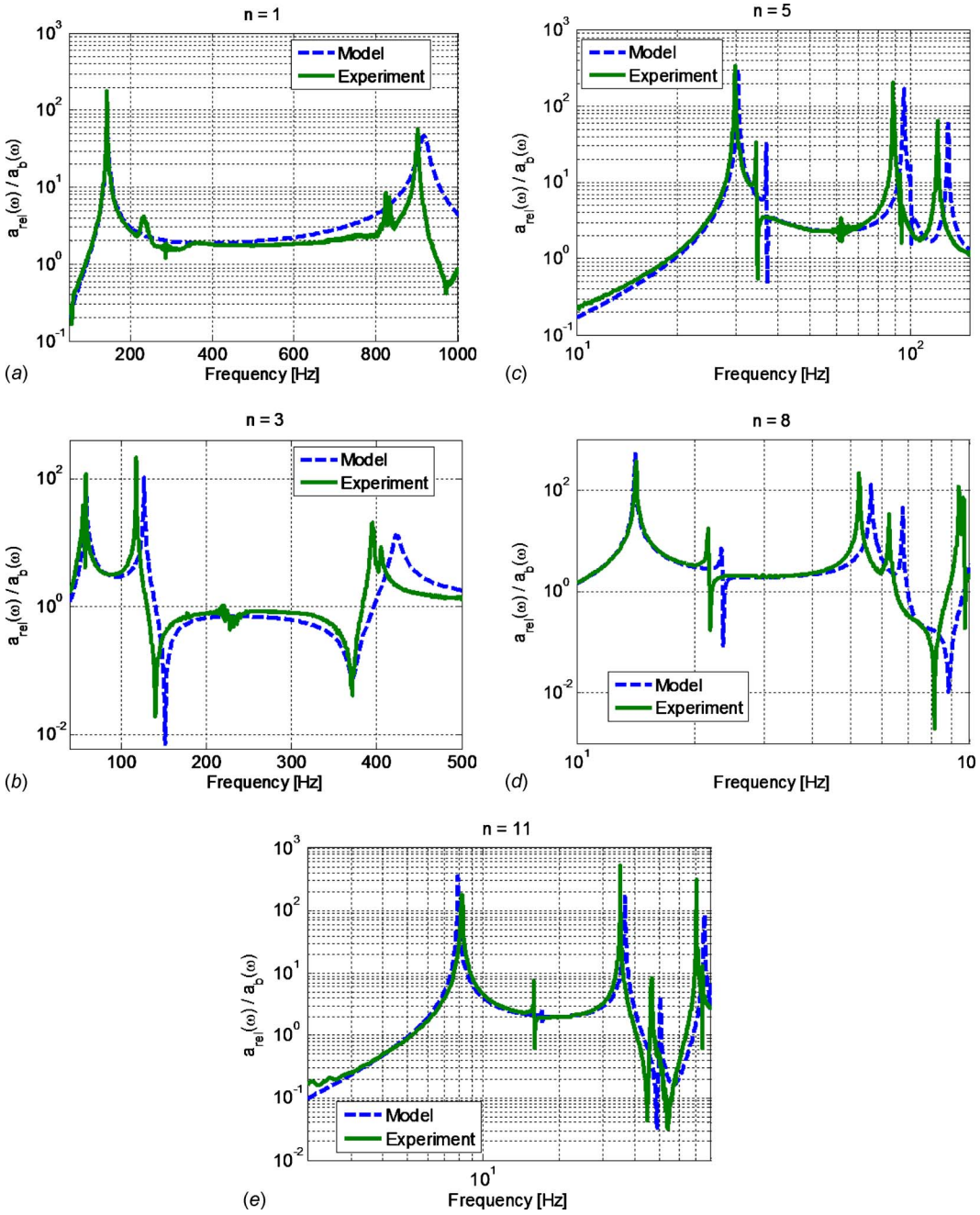

Fig. 9 Analytical predictions versus experimental measurements

In calculating the analytical results in Fig. 9, the values of Young's modulus and the density of the substrate were found in the material data sheet, and the link masses were calculated by multiplying the density by the volume of the links. The damping ratios were selected according to the thickness of the experimental frequency response function (FRF) peaks. The analytical predictions are close to the experimental measurements. The experiment shows that the actual natural frequencies are slightly lower than the model predictions. This small discrepancy is likely due to the fact that the links are not perfectly rigid. This flexibility translates to lower natural frequencies. Another possible reason for the difference is the fact that the last beam is about 10% longer than other beams. This extra length was considered as a tip mass in the analytical model, which in reality results in slight overestimations of the natural frequencies. That the experimental results match our predictions for the tip acceleration transfer function verifies that the natural frequencies and the mode shapes have both been predicted correctly. It also justifies the modeling assumptions, and the zigzag approach will, in fact, allow the production of MEMS harvesting devices with low natural frequencies compatible with ambient excitation.

9 Conclusion

Here, we proposed a new geometry to lower the frequency of a MEMS scale harvesting device without increasing its length, making the substrate device compatible with the frequency range of ambient vibrations. We developed an analytical method to calculate the natural frequencies and mode shapes of the proposed zigzag bilayered structure. The predictions of the analytical model were validated by Rayleigh's method results and experimental tests. The results from the analytical method confirm the possibil-

ity of designing a compact microscale energy harvesting device with a low fundamental natural frequency. Implementation of the proposed zigzag structure can reduce the first bending natural frequency by an order of magnitude and can bring it within the range of typical ambient vibrations.

The analysis developed here is based on assuming that each link behaves as an Euler–Bernoulli beam in bending and torsion, coupled by short links. Here, we assumed that the links between the beams are rigid, but we considered their mass in the model. Unlike the models used for frames, coupling torsion of beams, allowing for out of plane deformations, is considered.

The analytical study performed is of lower order and numerically more robust than using a finite element approach. Since the proposed method is relatively fast and accurate, it can be utilized for a future parametric analysis of the vibrations. The parametric studies can result in the characteristic curves, which are easier to use for vibration engineers. The design and the subsequent analysis presented here provide a low frequency substrate that can be used in energy harvesting studies for MEMS devices because the natural frequencies are of the order exhibited in most ambient energy signals.

Acknowledgment

This work was performed under the support of the U.S. Department of Commerce, National Institute of Standards and Technology, Technology Innovation Program, Cooperative Agreement No. 70NANB9H9007. This work was supported in part by the Institute for Critical Technology and Applied Science (ICTAS).

M.A.K. would like to thank Prof. Masoud Agah for his course on MEMS fabrication during which the idea of using the zigzag design occurred to the first author.

Nomenclature

b = width of the beams
GJ = torsional stiffness
h_p = thickness of the piezoelectric layer
h_s = thickness of the substructure
$k=GJ/EI_x$ = stiffness parameter
l = length of each of the beams
L = left transformation matrix
m_{tip} = mass of the tip
m_l = mass of the links
$M(x,t)$ = bending moment
$Q(x,t)$ = shear force
R = right transformation matrix
$T(x,t)$ = twist torque
$w_i(x)$ = out of plane deformation of the ith beam
x_{end} = x-coordinate of the free end
x^* = x-coordinate of the connection of two beams
Y_s = Young's modulus of the substructure
Y_p = Young's modulus of the piezoelectric layer
YI = bending stiffness
$\beta_i(x)$ = twist angle of the ith beam
ρ_p = density of the piezoelectric material
ρ_s = density of the substructure material
ρA = mass per unit length

References

[1] Beeby, S. P., Tudor, M. J., and White, N. M., 2006, "Energy Harvesting Vibration Sources for Microsystems Applications," Meas. Sci. Technol., **17**(12), p. R175.
[2] Anton, S., and Sodano, H., 2007, "A Review of Power Harvesting Using Piezoelectric Materials (2003–2006)," Smart Mater. Struct., **16**(3), p. R1.
[3] Arnold, D., 2007, "Review of Microscale Magnetic Power Generation," IEEE Trans. Magn., **43**(11), pp. 3940–3951.
[4] Cook-Chennault, K., Thambi, N., and Sastry, A., 2008, "Powering MEMS Portable Devices—A Review of Non-Regenerative and Regenerative Power Supply Systems With Special Emphasis on Piezoelectric Energy Harvesting Systems," Smart Mater. Struct., **17**(4), p. 043001.
[5] Priya, S., 2007, "Advances in Energy Harvesting Using Low Profile Piezoelectric Transducers," J. Electroceram., **19**(1), pp. 167–184.
[6] Priya, S., and Inman, D., 2008, *Energy Harvesting Technologies*, Springer, New York.
[7] Erturk, A., and Inman, D., 2008, "A Distributed Parameter Electromechanical Model for Cantilevered Piezoelectric Energy Harvesters," ASME J. Vibr. Acoust., **130**, p. 041002.
[8] Erturk, A., and Inman, D., 2008, "Issues in Mathematical Modeling of Piezoelectric Energy Harvesters," Smart Mater. Struct., **17**, p. 065016.
[9] Lu, F., Lee, H., and Lim, S., 2004, "Modeling and Analysis of Micro Piezoelectric Power Generators for Micro-Electromechanical-Systems Applications," Smart Mater. Struct., **13**(1), pp. 57–63.
[10] Jeon, Y. B., Sood, R., Jeong, J.-h., and Kim, S.-G., 2005, "MEMS Power Generator With Transverse Mode Thin Film PZT," Sens. Actuators, A, **122**(1), pp. 16–22.
[11] Kuehne, I., Marinkovic, D., Eckstein, G., and Seidel, H., 2008, "A New Approach for MEMS Power Generation Based on a Piezoelectric Diaphragm," Sens. Actuators, A, **142**(1), pp. 292–297.
[12] Zheng, Q., and Xu, Y., 2008, "Asymmetric Air-Spaced Cantilevers for Vibration Energy Harvesting," Smart Mater. Struct., **17**, p. 055009.
[13] Fang, H., Liu, J., Xu, Z., Dong, L., Wang, L., Chen, D., Cai, B., and Liu, Y., 2006, "Fabrication and Performance of MEMS-Based Piezoelectric Power Generator for Vibration Energy Harvesting," Microelectron. J., **37**(11), pp. 1280–1284.
[14] Shen, D., Park, J., Ajitsaria, J., Choe, S., Wikle, H., and Kim, D., 2008, "The Design, Fabrication and Evaluation of a MEMS PZT Cantilever With an Integrated Si Proof Mass for Vibration Energy Harvesting," J. Micromech. Microeng., **18**(5), p. 055017.
[15] Liu, J.-Q., Fang, H.-B., Xu, Z.-Y., Mao, X.-H., Shen, X.-C., Chen, D., Liao, H., and Cai, B. C., 2008, "A MEMS-Based Piezoelectric Power Generator Array for Vibration Energy Harvesting," Microelectron. J., **39**(5), pp. 802–806.
[16] Reilly, E., and Wright, P., 2009, "Modeling, Fabrication and Stress Compensation of an Epitaxial Thin Film Piezoelectric Microscale Energy Scavenging Device," J. Micromech. Microeng., **19**, p. 095014.
[17] Shen, D., Park, J., Noh, J., Choe, S., Kim, S., Wikle, H., and Kim, D., 2009, "Micromachined PZT Cantilever Based on SOI Structure for Low Frequency Vibration Energy Harvesting," Sens. Actuators, A, **154**(1), pp. 103–108.
[18] Lee, B., Lin, S., Wu, W., Wang, X., Chang, P., and Lee, C., 2009, "Piezoelectric MEMS Generators Fabricated With an Aerosol Deposition PZT Thin Film," J. Micromech. Microeng., **19**, p. 065014.
[19] Choi, W., Jeon, Y., Jeong, J., Sood, R., and Kim, S., 2006, "Energy Harvesting MEMS Device Based on Thin Film Piezoelectric Cantilevers," J. Electroceram., **17**(2–4), pp. 543–548.
[20] Karami, M. A., Yardimoglu, B., and Inman, D. J., 2010, "Coupled Out of Plane Vibrations of Spiral Beams for Micro-Scale Applications," J. Sound Vib., **329**(26), pp. 5584–5599.
[21] Barton, D. A. W., Burrow, S. G., and Clare, L. R., 2010, "Energy Harvesting From Vibrations With a Nonlinear Oscillator," ASME J. Vibr. Acoust., **132**(2), p. 021009.
[22] Rao, S. S., 2007, *Vibration of Continuous Systems*, Wiley, New York.
[23] Booker, J., and Kitipornchai, S., 1971, "Torsion of Multilayered Rectangular Section," J. Engrg. Mech. Div., **97**(5), pp. 1451–1468.
[24] Blevins, R., 1979, "Straight Beams," *Formulas for Natural Frequency and Mode Shape*, Krieger, Malabar, FL.
[25] Inman, D. J., 2001, "Distributed-Parameter Systems," *Engineering Vibrations*, Prentice-Hall, Englewood Cliffs, NJ.
[26] Meirovitch, L., 1967, "*Analytical Methods in Vibration*," Macmillan, London.
[27] Shames, I. H., and Dym, C. L., 2003, *Energy and Finite Element Methods in Structural Mechanics*, Taylor & Francis, New York.
[28] Ohashi, M., Nakamura, K., Hirao, K., Toriyama, M., and Kanzaki, S., 1997, "Factors Affecting Mechanical Properties of Silicon Oxynitride Ceramics," Ceram. Int., **23**(1), pp. 27–37.